Monthly Notices of the ROYAL ASTRONOMICAL SOCIETY

Mon. Not. R. Astron. Soc. **402,** 2321–2334 (2010) doi:10.1111/j.1365-2966.2009.16089.x

The origin of the Hubble sequence in ΛCDM cosmology

Andrew J. Benson[1★] and Nick Devereux[2★]

[1]*Mail Code 130-33, California Institute of Technology, Pasadena, CA 91125, USA*
[2]*Department of Physics, Embry-Riddle Aeronautical University, Prescott, AZ 86301-3720, USA*

Accepted 2009 November 20. Received 2009 November 19; in original form 2009 September 30

ABSTRACT

The GALFORM semi-analytic model of galaxy formation is used to explore the mechanisms primarily responsible for the three types of galaxies seen in the local universe: bulge, bulge+disc and disc, identified with the visual morphological types E, S0/a-Sbc and Sc-Scd, respectively. With a suitable choice of parameters the GALFORM model can accurately reproduce the observed local K_s-band luminosity function (LF) for galaxies split by visual morphological type. The successful set of model parameters is used to populate the Millennium Simulation with 9.4 million galaxies and their dark matter haloes. The resulting catalogue is then used to explore the evolution of galaxies through cosmic history. The model predictions concur with recent observational results including the galaxy merger rate, the star formation rate and the seemingly antihierarchical evolution of ellipticals. However, the model also predicts significant evolution of the elliptical galaxy LF that is not observed. The discrepancy raises the possibility that samples of $z \sim 1$ galaxies which have been selected using colour and morphological criteria may be contaminated with galaxies that are not actually ellipticals.

Key words: galaxies: elliptical and lenticular, cD – galaxies: evolution – galaxies: formation – galaxies: luminosity function, mass function – galaxies: spiral – galaxies: structure.

1 INTRODUCTION

The current paradigm, constrained in part by the K_s-band (hereafter K-band) luminosity function (LF) (e.g. Benson et al. 2003a), has galaxy discs forming through a combination of cold gas accretion (Weinberg et al. 2004) and feedback (Oppenheimer & Davé 2006), with bulges resulting from mergers (e.g. Barnes & Hernquist 1992; Hopkins et al. 2008; Masjedi, Hogg & Blanton 2008). Thus, the diversity of galaxy morphologies seen today represents the culmination of multiple evolutionary paths. These end points in galaxy evolution are captured in a taxonomy devised by Hubble (1936) and refined by de Vaucouleurs (1959) and de Vaucouleurs et al. (1991) that is based on the relative prominence of the stellar bulge and the degree of resolution of the spiral arms. Despite attempts to emulate this classification scheme using quantitative proxies such as colours (e.g. Strateva et al. 2001), concentration-asymmetry indices (e.g. Watanabe, Kodaira & Okamura 1985; Abraham et al. 1996; Bell et al. 2003), the Gini-M20 classifiers (Lotz, Primack & Madau 2004) and parametric methods involving bulge/disc decompositions (Schade et al. 1996; Ratnatunga, Griffiths & Ostrander 1999; Simard et al. 2002), there are no quantitative measures that uniquely segregate galaxies into the morphological groups represented by the de Vaucouleurs numerical T system (e.g. Graham & Worley 2008). Thus, proxies are merely a useful stopgap until the difficult and time-consuming task of assigning visible morphologies to the ever-growing number of catalogued galaxies can be accomplished.[1]

Fortunately, the time-consuming task of assigning visible morphologies has now been completed for the vast majority of nearby galaxies. The principal aim of this paper is therefore to use the K-band LF for nearby galaxies (Devereux et al. 2009) to constrain models of their formation and evolution. The K-band LF is of particular interest because of its relevance to understanding galaxy evolution in the context of lambda cold dark matter (ΛCDM) cosmology; at $z = 0$, the K-band LF traces the stellar mass accumulated in galaxies at a wavelength where interstellar extinction is minimal (Devereux, Becklin & Scoville 1987; Bell & de Jong 2000; Bell et al. 2003). Additionally, the functional forms for the K-band LFs distinguish between *bulge*-dominated and *disc*-dominated systems which suggests that at least two quite distinct galaxy formation mechanisms are at work to produce the diversity of morphological types seen in the local universe. Previous attempts to model the LFs in the context of hierarchical clustering scenarios (e.g. Cole et al. 2000; Benson et al. 2003a) have focused on the *Universal* or *Total* K-band LF, which is the sum over all galaxy types, because they are based on samples for which there are no pre-existing morphological assignments. In this paper, the K-band LFs are modelled for galaxies segregated by visible morphology in order to better understand

★E-mail: abenson@caltech.edu (AJB); devereux@erau.edu (ND)

[1]See the Galaxy Zoo Project, http://www.galaxyzoo.org/

Table 1. The table presents the mapping between morphological type and K-band B/T required for our best-fitting model to reproduce the relative abundances of each class in the interval $-23.5 < M_{\rm K} - 5\log_{10} h \leq -23$. Additionally, the final three columns show the percentage of galaxies in each class with $M_{\rm K} - 5\log h < -21$ and B/T less than the value indicated. For example, 80 per cent of bright S0-Sbc galaxies have a B/T less than 0.65.

Morphological class	B/T Range	B/T distribution 20 per cent	50 per cent	80 per cent
E	$0.92 < {\rm B/T_K} \leq 1.00$	0.99	1.00	1.00
S0-Sbc	$0.11 < {\rm B/T_K} \leq 0.92$	0.22	0.39	0.65
Sc-Scd	$0.00 \leq {\rm B/T_K} \leq 0.11$	0.00	0.01	0.05

(1) the origin and evolution of bulgeless disc galaxies, represented in the observable universe by Sc-Scd galaxies, (2) the role of secular processes in building the bulges of spiral (S0/a-Sbc) and lenticular galaxies and (3) the galaxy merger history that led to the formation of elliptical galaxies. Our analysis differs from that of Parry, Eke & Frenk (2009) in that the GALFORM model predictions are constrained by the observed K-band LFs for galaxies of different morphological type. Those model predictions are then compared with recent observational results including the type averaged galaxy merger rate and the type specific star formation (SSF) rate, both quantified as a function of redshift.

Observationally, there is a weak dependence of K-band bulge-to-total ratio (B/T) on visual morphology (Graham & Worley 2008) which is used in this paper to segregate the model galaxies into three broad groups representing the three types of galaxies seen in the local universe, namely bulge, bulge+disc and disc.[2] These three groups are identified with the visual morphological types E, S0/a-Sbc and Sc-Scd, respectively. Following Graham & Worley (2008), these three broad groups are identified in the models by adopting the range of B/T listed in Table 1. The table also indicates the distribution of B/T within each morphological class, illustrating that most disc galaxies (including S0's) have a rather low B/T. For example, 80 per cent of S0 and later type galaxies brighter than $M_{\rm K} - 5\log_{10} h = -21$ have B/T ≤ 0.54. If the magnitude limit is lowered to $M_{\rm K} - 5\log_{10} h = -19$, we find that 80 per cent of such galaxies have B/T ≤ 0.35. This is in agreement with the broad conclusion of Graham & Worley (2008) that most disc galaxies (including S0's) have low B/T (e.g. B/T $< 1/3$).

2 MODEL

The GALFORM semi-analytic model has been described most recently by Bower et al. (2006) and the reader is referred to that paper for a full description. In the model, galaxies consist of an exponential disc containing both gas and stars and a spheroidal stellar component – the morphology of the model galaxies is therefore determined by the relative amount of light in each component. A few key points regarding morphological evolution of model galaxies bear reiterating however:

(1) galaxies initially form through the cooling of gas from their surrounding dark matter halo. This gas is assumed to conserve its angular momentum during collapse and to therefore form a disc. As such, a galaxy formed in isolation will always be a pure disc galaxy unless it is sufficiently self-gravitating to become unstable.

(2) discs which become too self-gravitating become unstable to the formation of global perturbations and therefore destroy themselves. Instability is judged using the criterion proposed by Efstathiou, Lake & Negroponte (1982). For a disc to be stable it must satisfy

$$\frac{v_{\rm D}}{({\rm G}M_{\rm D}/R_{\rm D})^{1/2}} > \epsilon, \tag{1}$$

where v is the circular velocity of the disc at its half-mass radius, $R_{\rm D}$, and $M_{\rm D}$ is the mass of the disc. The value of ϵ for purely stellar discs was found to be 1.1 by Efstathiou et al. (1982), although lower values may be appropriate for gas-rich discs (Christodoulou, Shlosman & Tohline 1995). We treat ϵ as a free parameter. If a disc is deemed to be unstable according to this criterion, the disc is destroyed, with any stars and gas present forming a spheroidal system in which the gas is then rapidly turned into stars.[3] The end result is a purely spheroidal (also known as elliptical) system.

(3) mergers between galaxies can also create a spheroidal component. Galaxy–galaxy mergers are driven by dynamical friction on a satellite galaxy (and its halo) orbiting in a larger dark matter halo. Merging time-scales are computed using a modified form of Chandrasekhar's dynamical friction equation (Lacey & Cole 1993). The time-scales are scaled by $\tau^0_{\rm mrg}$, a parameter of the model, to allow some adjustment of merger rates. Mergers are split into the following two categories.

(a) *Minor Mergers*: these are mergers with $M_2/M_1 < f_{\rm ellip}$ where M_1 and $M_2 < M_1$ are the baryonic masses of the galaxies involved in the merger and $f_{\rm ellip}$ is a parameter of the model (see below). In a minor merger, the stars from the secondary (lower mass) galaxy are added to the spheroidal component of the primary (more massive) galaxy while any gas from the secondary is added to the disc of the primary. A galaxy can therefore grow a spheroidal component through the cumulative effects of many minor mergers.

(b) *Major Mergers*: these are mergers with $M_2/M_1 \geq f_{\rm ellip}$ and cause the destruction of any pre-existing stellar discs, such that all stars from the merging galaxies become part of the spheroidal component in the merger remnant. The fate of any gas in the merging galaxies also depends on the merger mass ratio.

(i) If $M_2/M_1 < f_{\rm burst}$, where $f_{\rm burst}$ is a parameter of the model, then the merger does not trigger a burst of star formation and any gas forms a disc in the merger remnant (and may subsequently form stars in that disc).

[2]In principle, other outputs from the model could be used to provide additional information on morphological type. However, Graham & Worley (2008) show that bulge/disc flux ratio is the most useful discriminant as it varies more, as a function of morphological type, than other indicators, such as bulge/disc size ratio, for example.

[3]Since the treatment of this instability process in semi-analytic models is somewhat uncertain, an alternative and less dramatic implementation is presented in the Appendix A2. The results do not change the qualitative conclusions of this paper.

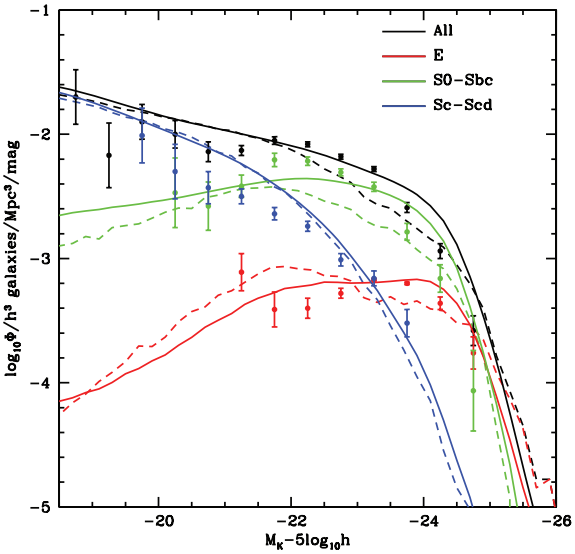

Figure 1. Morphologically selected K-band LFs for the best-fitting model (Table 2) are shown by solid lines and are compared to the observed LFs of Devereux et al. (2009) shown by the points. Colours indicate morphological class as indicated by the key in the figure. Galaxies are split into three morphological classes according to Table 1. For reference, dashed lines show results from the Bower et al. (2006) model (i.e. without the parameter modifications introduced in this work) using the same cuts on B/T to define morphological classes.

Table 2. Parameters of the best-fitting model.

Parameter	Value Best fit	Value Bower et al. (2006)
ϵ	0.8	0.8
$\tau_{0\mathrm{mrg}}$	3.0	1.5
f_{ellip}	0.15	0.3
f_{burst}	0.2	0.1
$V_{\mathrm{hot,disc}}$	485 km s^{-1}	485 km s^{-1}
$V_{\mathrm{hot,burst}}$	300 km s^{-1}	485 km s^{-1}

(ii) If $M_2/M_1 \geq f_{\mathrm{burst}}$, then the merger triggers a burst of star formation and any gas present in the merging galaxies is turned into stars on a short time-scale and becomes part of the spheroidal component of the merger remnant.

(4) Once a spheroidal component has formed, subsequent gas cooling can cause a disc to regrow around the spheroid, resulting in a galaxy with intermediate B/T.

(5) The model includes supernovae feedback which is assumed to drive gas out of a galaxy at a rate proportional to the star formation rate: $\dot{M}_{\mathrm{out}} = \beta \dot{M}_\star$, where $\beta = (V_{\mathrm{hot}}/V)^{\alpha_{\mathrm{hot}}}$, V is the circular speed of the galaxy and V_{hot} and α_{hot} are parameters of the model. V_{hot} may differ for quiescent star formation in discs and bursts of star formation.

The Bower et al. (2006) model was not constructed using morphological data as a constraint. Our initial goal, therefore, is to adjust the parameters of the Bower et al. (2006) model so that it reproduces the observed morphologically segregated LFs of Devereux et al. (2009), shown in Fig. 1. A search for an alternative set of values for the six model parameters that match the observed morphologically selected LFs yielded the values listed in Table 2. The best-fitting model LFs (lines) are compared with the observed LFs from Devereux et al. (2009) (points) in Fig. 1. Morphological class is indicated by colour in the figure. The relative abundance of each type in the model is forced to agree with the data in the interval $-23.5 < M_{\mathrm{K}} - 5\log_{10} h \leq -23.0$ (this is how the mapping between B/T and morphological class listed in Table 1 was determined) but the morphological mix is not enforced outside this magnitude range. Also shown, for reference, are the results from the unmodified Bower et al. (2006) model (dashed lines). The comparison shows that the model results are quite similar.

The model LFs for ellipticals, lenticulars and bulge-dominated spirals are peaked and decline toward both higher and lower luminosities. In contrast, the Sc-Scd class continues to rise towards low luminosities and dominates the total LF for $M_{\mathrm{K}} - 5\log_{10} h > -22$. The black line and points indicate the total (i.e. all morphological types) LF. Not surprisingly, the model prediction here is also in good agreement with the data. This is to be expected however, since the model parameters are optimized to yield a satisfactory representation of the observed LFs for each of the three broad morphological types and the total LF is just the sum of these. Additionally, Bower et al. (2006) have already demonstrated that the model can fit the observed total K-band LF. The parameters yielding the best-fitting model (Table 2) are similar to those adopted by Bower et al. (2006): disc instability estimates are unchanged, but the rate of galaxy merging has been reduced by a factor of 2, a lower mass ratio in mergers is required to disrupt stellar discs, a higher ratio is required to trigger a burst, while the feedback in bursts, but not discs, has been weakened.

3 RESULTS

Having found a successful set of model parameters, they are used to populate the Millennium Simulation (Springel et al. 2005) with galaxies. To do this, dark matter halo merger trees are extracted from the Millennium Simulation using the techniques described by Harker et al. (2006). The trees are then populated with galaxies in the manner described by Bower et al. (2006), but using the model parameters found in the previous section. This results in a catalogue of 9.4 million galaxies and their dark matter haloes. The catalogue provides the magnitudes, morphologies and other physical characteristics of all the galaxies, including their evolution through cosmic history. The catalogue can therefore be used to explore galaxy evolution. Our goal is to reveal the key physical processes at work that produce the three broad types of galaxies in the observable universe, namely bulges, bulges+discs and discs. The resolution of the Millennium Simulation, as in any N-body simulation, is limited. In Appendix A1, a study of the effects of resolution demonstrates that the morphological features of the model galaxies are well converged at the resolution of the Millennium Simulation.

3.1 Trends with morphological class

3.1.1 Dark matter halo properties

The relationship between galaxy luminosity and dark matter halo mass is illustrated in Fig. 2 as a function of morphological type. The solid lines in Fig. 2 indicate the mass of the halo in which a galaxy formed, defined here following Cole et al. (2000) such that haloes are labelled as 'reforming' each time they undergo a doubling of their mass. As may be expected, there is a correlation between galaxy luminosity and the median mass of the dark matter halo in which such galaxies formed. The slope of the relation is

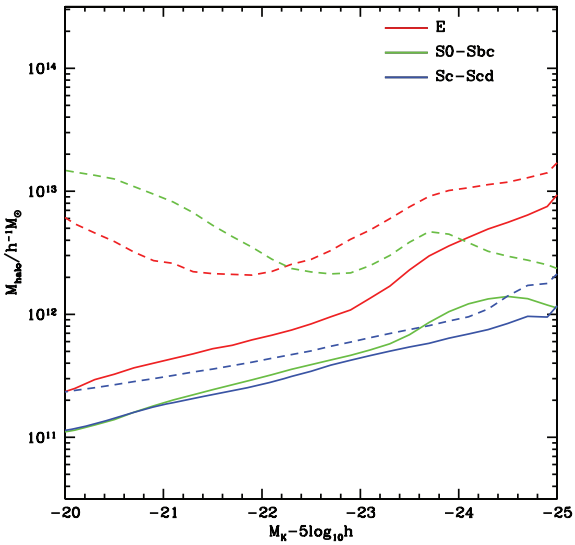

Figure 2. The median halo mass in which galaxies formed (solid lines) and the mass of their current halo at $z = 0$ (dashed lines) as a function of K-band luminosity and morphological class (colour coding as in Fig. 1). The current halo mass is the same as the mass of the halo in which the galaxy formed for central galaxies but may be significantly larger for satellite galaxies.

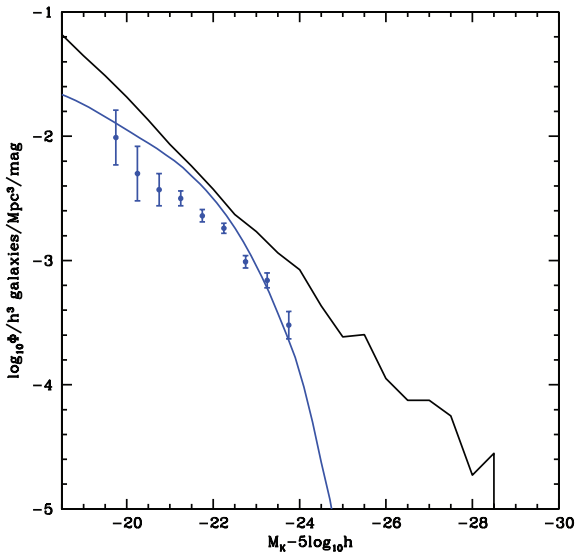

Figure 3. The Sc-Scd K-band LF (blue line and points) versus the median formation halo mass function (black line) scaled by a M/L.

quite flat however, showing a range of a factor of ∼20 in halo mass over a factor of ∼100 range in luminosity.

There is little dependence of median formation halo mass on morphological type, except for the E class which form in haloes around a factor of ∼3 more massive for a given luminosity. This may be expected for the E class if such galaxies are built up via merging rather than continuous gas accretion. To attain the same luminosity as its accretion-fuelled counterpart, a merger-built galaxy must form in a more massive halo so that the rate of merging will be enhanced.

The dashed lines in Fig. 2 indicate the mass of the dark matter halo in which a galaxy lives at $z = 0$. In the case of satellite galaxies, this is the mass of the isolated dark matter halo in which they orbit, *not* the mass of the subhalo within which they reside. The difference between the dashed and solid lines is therefore indicative of how much mass has accumulated in the dark matter halo since galaxies formed. Dark matter haloes may grow through mergers of satellites and by accretion. With the exception of Sc-Scd galaxies, the mass of the halo in which galaxies live at $z = 0$ greatly exceeds the mass of halo in which they formed, particularly for the lower luminosity systems (a simple consequence of the fact that the low-mass haloes in which these faint galaxies form are highly likely to be subsumed into much more massive haloes by $z = 0$ by becoming satellites of those haloes).

Interestingly, Sc-Scd galaxies of all luminosities occupy dark matter haloes that are only about a factor of 2 more massive than those in which they formed. Thus, disc-dominated galaxies must have avoided major mergers by virtue of living in dark matter haloes having rather quiet merging histories. There are a wide variety of possible merger histories for haloes of a given mass (Stewart et al. 2008) including some fraction which will have avoided major mergers. It is known that haloes in low-density environments experience lower merger rates than their counterparts in high-density environments (Fakhouri & Ma 2009) and so are more likely to have a quiet merger history. Thus, Sc-Scd-type galaxies are distinguished from the other morphological types having formed preferentially in low-density environments. 65 per cent of Sc-Scd galaxies brighter than $M_K - 5\log_{10} h = -20$ are central galaxies, i.e. they are the most massive galaxy in their halo, and they grow primarily through gas accretion and not mergers. Consequently, the Sc-Scd K-band LF has a similar slope to the median formation halo mass function as illustrated in Fig. 3.

3.1.2 Time-scales

While interesting from a theoretical standpoint, dark matter halo masses cannot be easily measured for most galaxies. [Although weak lensing (Mandelbaum et al. 2006) and clustering (Mandelbaum et al. 2009) measures can constrain halo mass for classes of galaxies.] Greater utility is provided by examining observable quantities more directly related to the galaxies themselves, beginning with time-scales.

Fig. 4 shows the median stellar mass-weighted age of galaxies, defined as

$$\langle t_{\rm age}\rangle = \frac{\int_0^{t_0}(t_0 - t)\dot{\rho}_\star(t){\rm d}t}{\int_0^{t_0}\dot{\rho}_\star(t){\rm d}t}, \qquad (2)$$

where t_0 is the current age of the Universe and $\dot{\rho}_\star(t)$ is the star formation rate in a galaxy at time t, split by morphological type as a function of their K-band magnitude. Disc-dominated galaxies (blue line) are distinguished once again, this time by hosting a uniformly much younger stellar population than any other morphological type. This suggests that disc galaxies of all luminosities have been continuously forming stars since their formation which the model reveals is at a rate that is proportional to the baryonic mass of the galaxy. In contrast, the ellipticals, lenticulars and bulge-dominated spirals contain much older stellar populations with median ages of 10 Gyr. This does not mean that the galaxies formed 10 Gyr ago, merely that the stars now dominating the baryonic mass of the galaxies typically formed at that time. As we shall see in Section 3.1.4, massive ellipticals were actually assembled much more recently.

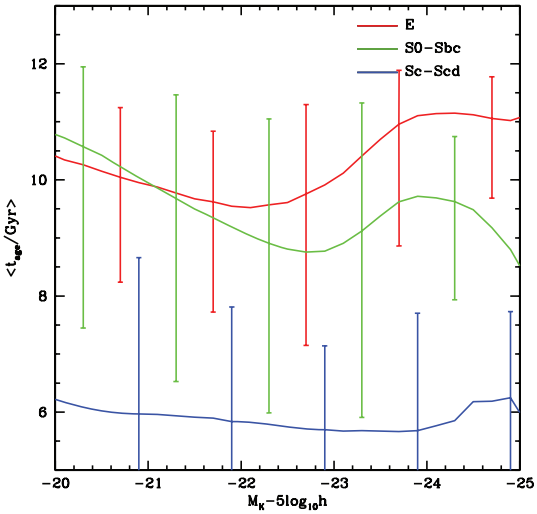

Figure 4. The stellar mass-weighted age of galaxies as a function of K-band magnitude and morphological class (colour coding as in Fig. 1). Solid lines indicate the median ages for galaxies in each morphological class while error bars indicate the $\pm$ 1σ interval of the distribution of ages.

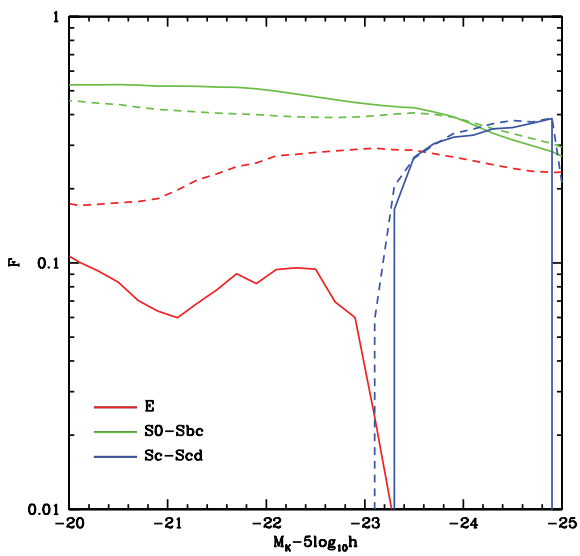

Figure 5. The fraction of a galaxy's bulge mass which was made in the most recent burst of star formation (solid lines) and disc instabilities (dashed lines) as a function of K-band magnitude for each morphological class (colour coding as in Fig. 1).

3.1.3 Bursts and bulge formation

Fig. 5 examines the fraction of a galaxy's bulge mass that was made in the most recent burst of star formation (solid lines) and the fraction formed through disc instabilities (the remainder being made through minor or major mergers). Interestingly, ∼30–50 per cent of the bulge mass in lenticulars and bulge-dominated spirals (S0/a-Sbc) resulted from disc instabilities with the remainder created in the most recent burst of star formation, which occurred ≤10 Gyr ago, that itself could have been triggered by a disc instability or a merger. Unfortunately, there is no way to distinguish between the two possibilities in this figure. The importance of these processes is greatly diminished in elliptical galaxies, because they do not possess discs[4] and in disc-dominated Sc-Scd galaxies, because they have small or non-existent bulges.[5]

3.1.4 Formation and assembly redshift distributions

Fig. 6 shows the distribution of star formation redshifts, $z_\star$, and assembly redshifts, $z_{\rm assem}$. The star formation redshift for a galaxy is defined to be the redshift at which half of the final stellar mass of the galaxy has been formed. The assembly redshift is the redshift at which half of the final stellar mass has been assembled into a single progenitor. Clearly for a given galaxy, $z_{\rm assem} < z_\star$. The most striking feature of these distributions is that the most luminous $-25 \leq M_{\rm K} - 5\log_{10} h \leq -24$ elliptical galaxies have a median star formation redshift $z_\star \sim 3$ while the median assembly redshift is much lower $z_{\rm assem} \leq 3$. This clearly shows that such galaxies are formed almost entirely through the merging of pre-existing systems that formed at higher redshift. The difference between star formation and assembly times diminishes for lower luminosity ellipticals, suggesting fewer mergers. Also, the stellar population is younger in lower luminosity ellipticals compared to their more luminous counterparts by ∼1 Gyr. Since the other morphological types (S0-Sbc) show remarkably little difference between their star formation and assembly redshift distributions, it is primarily the luminous ellipticals, $-25 \leq M_{\rm K} - 5\log_{10} h \leq -24$, whose growth is dominated by the delivery of pre-formed stars via mergers that happened recently, since $z \sim 3$.

The star formation and assembly redshifts are virtually identical for lenticular and spiral galaxies (S0-Scd) which suggests that major mergers do not play an important role in the evolution of these galaxy types. The $z_\star$ distributions are strongly peaked at low redshifts for the disc-dominated Sc-Scd galaxies. Thus, the models indicate that they should contain the youngest stellar populations with ages ≤6 Gyr. On the other hand, the $z_\star$ distributions for lenticular and bulge-dominated spirals become broader with decreasing luminosity suggesting a heterogeneous group with stellar populations spanning a wide range in age.

4 DISCUSSION

In order to understand both the trends found in Section 3 and the morphological evolutionary paths of galaxies, we examine formation tree diagrams such as Fig. 7. These show the detailed formation

[4]The dashed lines reflect the mass of stars that were formed through disc instabilities in *all* progenitors. Thus, the dashed red-line indicates that disc instabilties may have been an important mechanism for the progenitors of today's ellipticals. We note that the fraction of an elliptical's mass which formed as a result of disc instability events is sensitive to the details of the treatment of such instabilities in our model. With our standard treatment, on average 29 per cent of the spheroid mass in bright ($M_{\rm K} - 5\log_{10} h < -23$) ellipticals is made via disc instability events. Using a more moderate treatment of instability events in which a minimal amount of disc is converted into spheroid (see Appendix A2), this number is reduced to 9 per cent. These fractions are relatively insensitive to the resolution of the merger trees. The resolution study described in Appendix A1 indicates that they change by only 3 per cent for the brightest ellipticals as the resolution of the merger trees is increased by a factor of 16. For the faintest ellipticals shown (which are closer to the resolution limit of our calculations), the fraction changes by only 7 per cent with the same increase in resolution.

[5]However, the models do indicate that disc instabilities may be an important bulge formation mechanism in the luminous, $M_{\rm K} - 5\log_{10} h < -23$ mag, Sc-Scd galaxies.

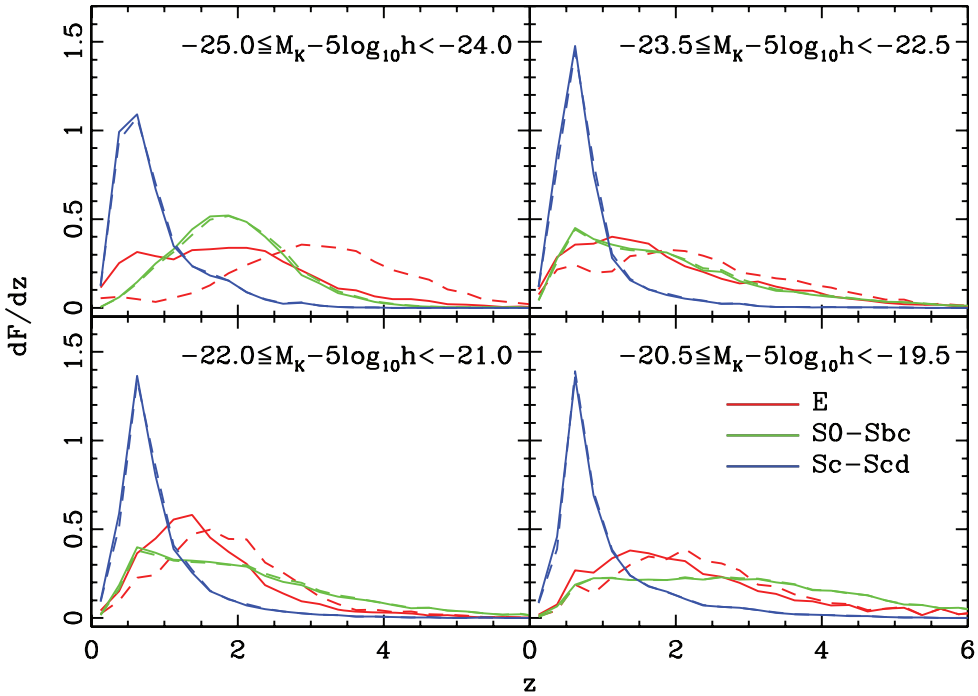

Figure 6. The normalized distributions of $z_\star$ (the redshift at which half of a galaxy's final number of stars were formed; dashed lines) and $z_{\rm assem}$ (the redshift at which half of the galaxy's final stellar mass was assembled into a single progenitor; solid lines) are shown split by morphological class (colour coding as in Fig. 1). Each panel corresponds to a different K-band magnitude interval as indicated in the panel. The distribution is normalized such that the integral under the curve is unity.

history of individual galaxies and therefore provide a more detailed examination of morphological evolution. The tree shown in Fig. 7 is for a luminous elliptical galaxy. As expected from the results of Section 3, this galaxy shows significant merging activity. There is a clearly identifiable main progenitor which has been a pure elliptical since $z \approx 0.5$. Half of the stars in the final galaxy were formed by $z = 3.75$ but were not assembled into a single galaxy until $z = 0.26$. Approximately, one-quarter of the stars in the galaxy were formed as a result of a burst triggered by a disc instability event which occurred at $z \approx 5$.

In Figs 8–10, we show tree diagrams for randomly selected galaxies in the E, S0/a-Sbc and Sc-Scd classes for a range of luminosities. (Note that the vertical axis of each plot is adjusted to stretch from $z = 0$ to the earliest redshift at which the galaxy has an identifiable progenitor.) The E class shows a clear transition from forming via multiple mergers in the high-luminosity regime to forming via disc instabilities in the low-luminosity regime. [A disc instability event in these diagrams is apparent as the solid (main progenitor) blue (disc) line drops to zero while the solid green and red lines jump to larger values.] These low-luminosity ellipticals start out as discs, gradually converting their gas into stars. Eventually, the disc becomes gravitationally unstable, triggering a burst and converting all stars and gas into a spheroid. The galaxy evolves passively after this time.

It is apparent that the number of progenitors is greatly reduced for the lower luminosity galaxies.[6] This is apparent for all morphological types except for the Sc-Scd class and is a consequence of the shape of the galaxy mass function in systems of differing halo mass (e.g. Benson et al. 2003b) – for the most massive haloes, the galaxy mass function is a very steep function of halo mass, such that there are many more galaxies of slightly lower mass with which the central galaxy can merge. For lower mass haloes, the galaxy mass function is shallower, yielding relatively fewer galaxies of lower mass. This results in fewer galaxies with which to merge and fewer progenitors. The shape of the galaxy mass function in our model arises because of supernovae feedback which is relatively stronger in lower mass haloes.

The S0/a-Sbc class has a much quieter history. Only the most luminous examples $M_{\rm K} - 5\log_{10} h \leq -25$ are involved in a few significant mergers. Lower luminosity systems experience periods of early growth characterized by multiple disc instability events that cause the disc mass to rise and then fall sharply. More recent growth, since $z \sim 2$, occurs when the disc has stabilized and is able to form stars quiescently until the gas supply is exhausted, typically between $z = 1$ and 2 for the lower luminosity systems and $z \sim 0$ for the luminous systems.

The Sc-Scd class has the most uneventful formation history of all. This is, of course, obvious from the fact that this class is defined to have almost no spheroidal component. These galaxies must therefore have experienced no significant instability or merger events. The tree diagrams of Fig. 10 show that this type of galaxy is characterized by steady star formation in a disc fuelled by cosmic infall, which continues either until $z = 0$, or until the galaxy becomes a satellite and therefore loses its gas supply.

[6]Galaxies of luminosity similar to that in panel d of this figure are affected by the resolution limit of the simulation as the haloes that they occupy typically contain around 50 particles, preventing their lower mass progenitors from being resolved. For galaxies of luminosity comparable to that in panel c (and brighter galaxies), resolution is not an issue – they inhabit haloes typically containing 500 particles, sufficient to permit many lower mass progenitor haloes to be resolved in the simulation.

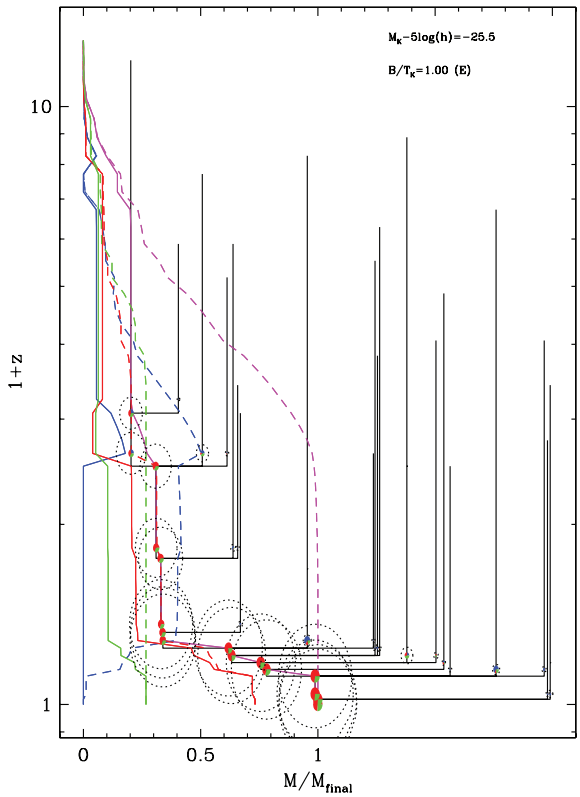

Figure 7. A formation tree diagram for a single galaxy identified at $z = 0$. The K-band magnitude and B/T of the galaxy at $z = 0$ are shown in the upper right-hand corner. The y-axis plots redshift, while the x-axis plots stellar mass relative to that of the $z = 0$ galaxy. The small pie charts indicate the final galaxy and any progenitor galaxies (shown down to progenitors with a mass of 0.1 per cent of the final galaxy). Black lines connecting galaxies indicate mergers between galaxies. The radius of each pie chart is proportional to the cube root of the stellar mass of the galaxy, while the segments of the pie chart show the relative fractions of stars in the galaxy's disc (blue) and bulge (red for stars formed by or brought in by mergers, green for stars formed or brought in by disc instabilities). The dotted circles around each galaxy are proportional to $(\Omega_b/\Omega_0)M_h$ and so will coincide with the size of the galaxy pie chart if a galaxy has succeeded in converting all available baryons in its halo into stars. Coloured lines indicate the total stellar mass (magenta) as well as that in the disc (blue), bulge (mergers) (red) and bulge (instabilities) (green) as a function of redshift. Solid lines show masses in the most massive progenitor, while dashed lines show the mass summed over all progenitors.

4.1 The merger history as a function of morphological type

Fig. 11 illustrates the merger history as a function of morphological type. $F(z)$ is the fraction of galaxies with mass $>2.5 \times 10^{10}\,\mathrm{M}_\odot$ (corresponding to $M_K - 5\log_{10} h \leq -22.7$) that have undergone a major merger ($M_2/M_1 > 0.25$) within the past 1 Gyr. These selection criteria allow a direct comparison with the observationally determined rates of Jogee et al. (2009) and López-Sanjuan et al. (2009). Galaxies are segregated according to their $z = 0$ morphology and the reported merger fractions resulted from integrating their respective merger trees over z. The model predicts an average merger fraction integrated over all galaxy types of ∼2 per cent which compares favourably with the observed lower limit to the major merger fraction for the sample S1 of Jogee et al. (2009) and the merger fraction measured at $z = 0.6$ for a slightly more luminous sample by López-Sanjuan et al. (2009). The model reveals that the merger rate is highest for elliptical galaxies; ∼8 per cent of ellipticals at $z = 0$ resulted from a major merger that occurred in the past 1 Gyr. The model elliptical merger rate is significantly higher than the merger rate estimated by Masjedi et al. (2008) for a sample of luminous red galaxies in close pairs. The model elliptical merger rate predicts significant evolution of the elliptical LF, as discussed in more detail in the next section. Very few of the $z = 0$ lenticular and (S0/a-Sbc) spiral galaxies, and none of the Sc-Scd disc galaxies, resulted from a major merger. Thus, the model predicts that Sc-Scd galaxies exist in the local universe because they have not been involved in any collisions.

We compare our predicted merger rates with other recent attempts to measure this quantity from either N-body simulations of dark matter or from semi-analytic models of galaxy formation. Before doing so, we remind the reader that our merger rate is that of galaxies, and so there is no reason to expect it to coincide with rates of, for example, dark matter halo merging or dark matter subhalo destruction (both of which are commonly measured quantities). In particular, Stewart et al. (2009) examined the rates of both halo merging (when a halo first crosses the virial radius of a larger halo, thereby becoming a subhalo) and subhalo destruction (when a subhalo loses 90 per cent of its mass) in an N-body simulation of dark matter. Stewart et al. (2009) find merger rates which increase monotonically with increasing redshift, in disagreement with our own findings. However, we caution that these results are based purely on dark matter properties (with a simple, redshift-dependent mapping of galaxy luminosity to dark matter halo mass) and so do not measure the same quantity as presented in this work. Similar results were found by Genel et al. (2009). On the other hand, Bertone & Conselice (2009) find merger fractions comparable to ours, with a broad peak around $z = 1.5$ and a gradual decline towards higher redshifts. The agreement is not surprising, however, as they derive merger rates from a semi-analytic model similar to the one used here.

4.2 The evolution of the elliptical galaxy luminosity function

The model predicts significant evolution of the elliptical galaxy K-band LF as illustrated in Fig. 12. The LF at each redshift has been k-corrected and further corrected for passive evolution to $z = 0$ so that the LFs may be compared on an equal basis. Within the GALFORM model, k-corrections and passive evolution can be computed precisely. The model predicts the full spectral energy distribution (SED) of each galaxy and so we can simply shift the filter to the galaxy rest frame and compute the absolute magnitude which will then automatically include the k-correction. For passive evolution, the model predicts the mix of stars in each galaxy at each redshift, including their distribution of ages and metallicities. To compute the magnitude of the galaxy at $z = 0$ assuming passive evolution (i.e. no further star formation), we simply artificially increase the ages of these stars by the look-back time to the current redshift and then sum their SEDs to give the net SED of the galaxy passively evolved to $z = 0$. The passively evolved magnitude of the galaxy is then trivially found by integrating under the appropriate filter response function. Our k- and evolution corrections are, at least at low redshifts, in reasonable agreement with those determined observationally by Bell et al. (2003). For example, in the K band at $z = 0.5$ we find k- and evolution corrections of approximately $k = -0.75$ and $e = 0.55$, to be compared to $k = -1.05 \pm 0.15$ and $e = 0.4$ from Bell et al. (2003).

Fig. 12 shows that the space density goes up at the high-luminosity end and down at the low-luminosity end as the redshift decreases. These evolutionary changes have been quantified in Table 3 in terms of the Schechter parameters ϕ_*/h^3, $M_* - 5\log_{10} h$

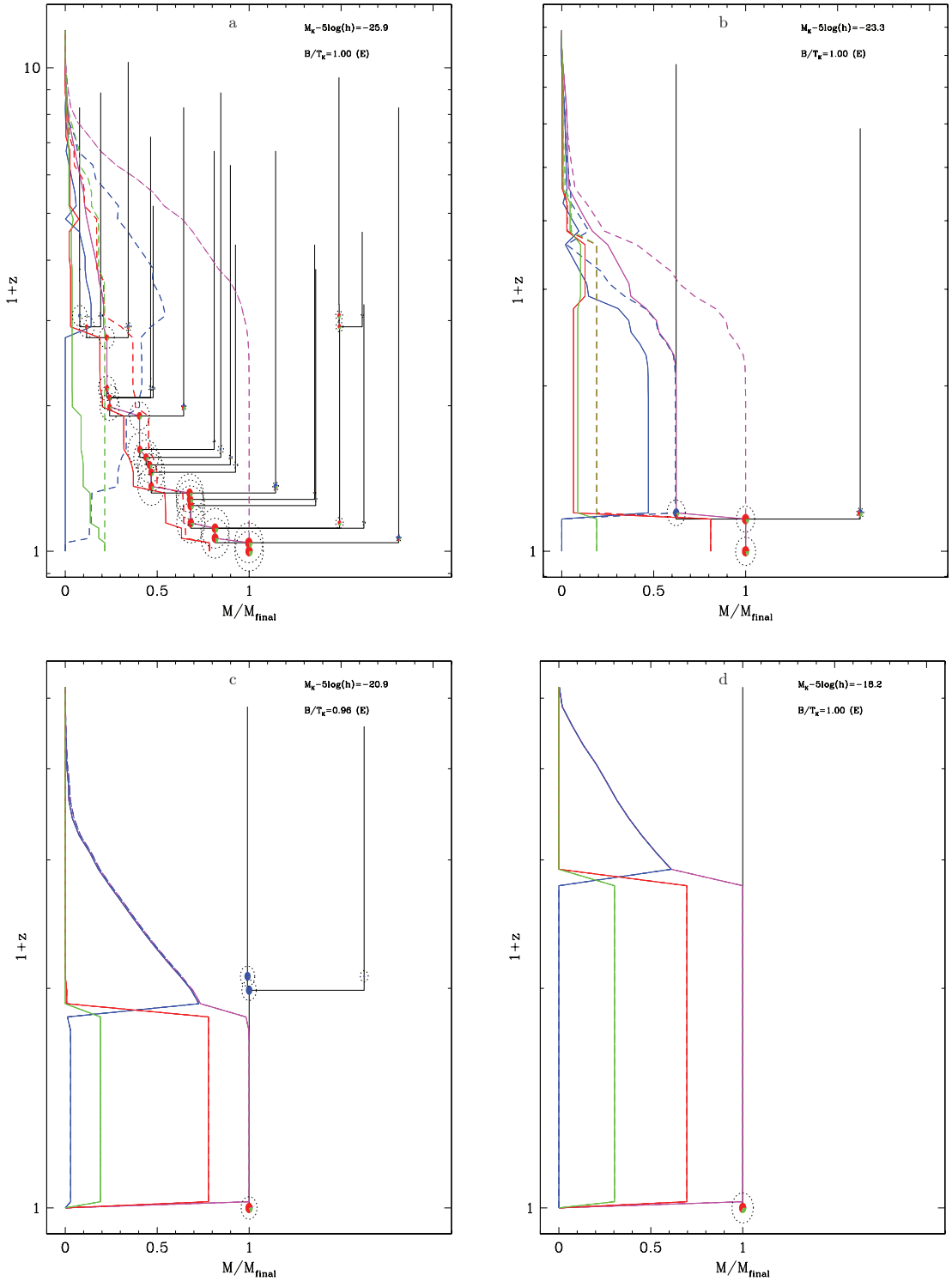

Figure 8. Formation tree diagrams for elliptical galaxies shown for four different magnitudes as indicated in the panels.

and α. The model results indicate that the mass build-up of ellipticals is reflected in the K band mostly through the large ∼226 per cent increase in ϕ_*/h^3 since $z = 1$, and a small, 0.2 ± 0.1 mag, brightening of $M_* - 5\log_{10} h$.

Parametrizing the LFs allows the luminosity density j to be calculated by integration as

$$j = \int \phi(M) 10^{0.4(\mathrm{M}_\odot - M)}\, \mathrm{d}M, \tag{3}$$

where $\mathrm{M}_\odot$ is the absolute magnitude of the Sun, corresponding to 3.32 mag at K (Bell et al. 2003). The luminosity density is important as it can provide a constraint on the mass density of stars in galaxies, given a mass-to-light ratio (M/L). The total K-band luminosity density at each redshift was calculated by integrating equation (3) over the interval $-25 \leq M_K - 5\log_{10} h \leq -19$ mag and the results are summarized in Table 3. These values indicate that the luminosity density, or equivalently, the mass density has increased by about a

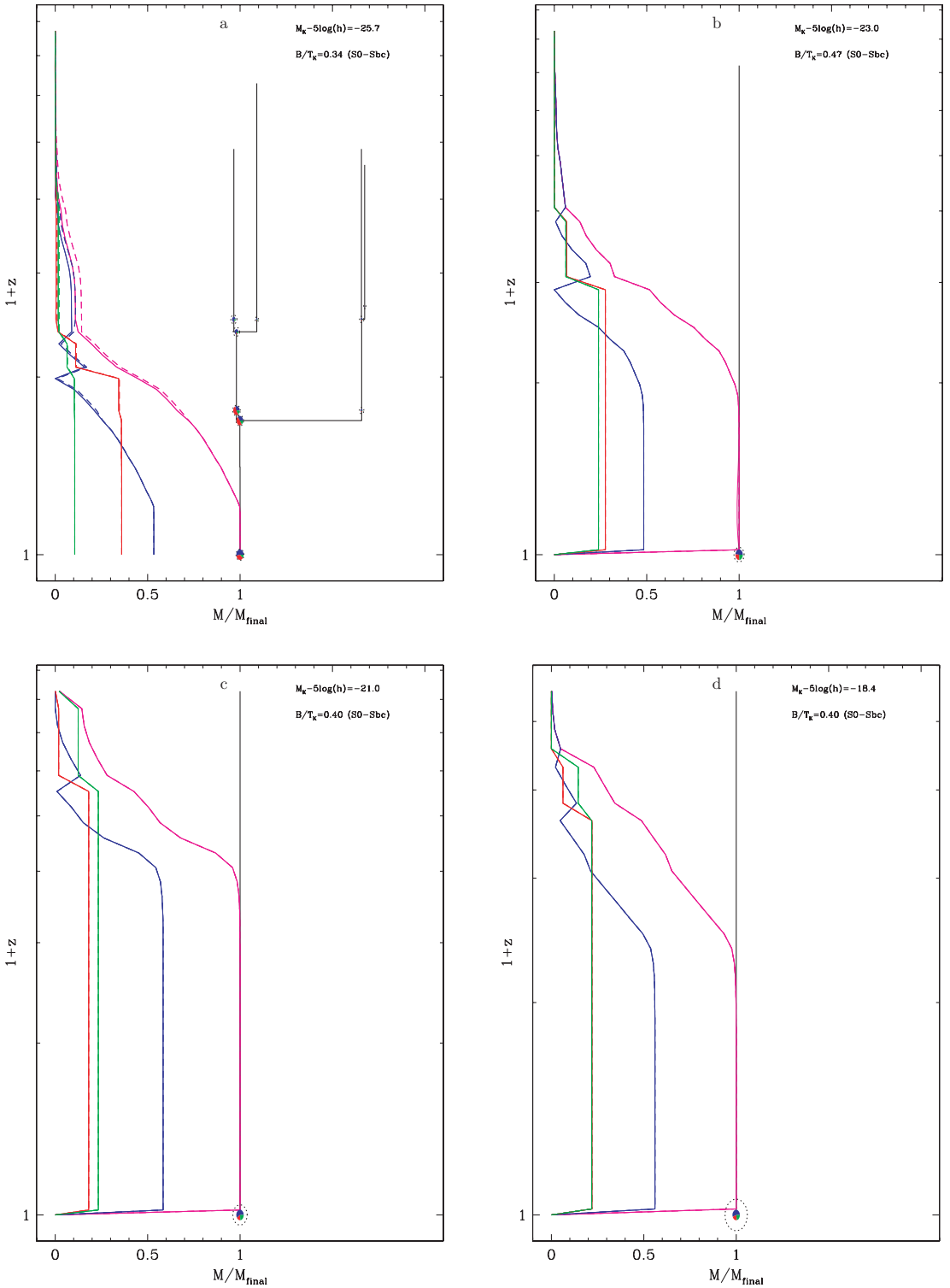

Figure 9. Formation tree diagrams for S0-Sbc galaxies shown for four different magnitudes as indicated in the panels.

factor of 2.4 since $z = 1$. The predicted evolution since $z = 2$ is even more dramatic. These model results concur in general with recent observational results suggesting that the stellar mass contained within the red galaxy population has at least doubled since $z \sim 1$ (Bell et al. 2004; Blanton 2006; Willmer et al. 2006; Brown et al. 2007; Faber et al. 2007).

Our model results further indicate that the mass density of luminous ellipticals grows at the expense of their lower luminosity counterparts causing the faint end slope to turn downwards with decreasing redshift. Such low-luminosity ellipticals are presumably satellites of their more luminous counterparts; they are difficult to detect observationally with current technology and contribute

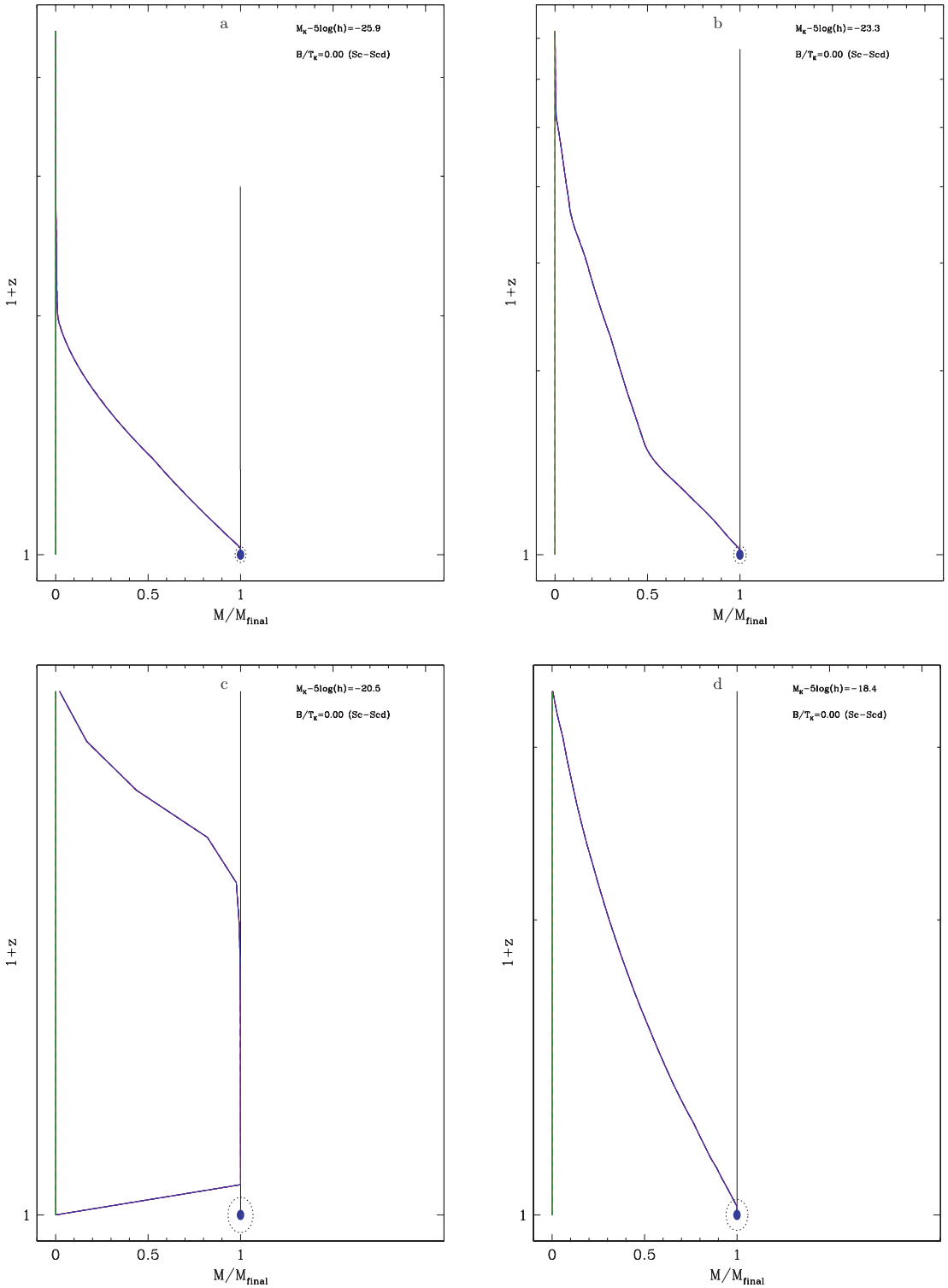

Figure 10. Formation tree diagrams for Sc-Scd galaxies shown for four different magnitudes as indicated in the panels.

negligibly to the luminosity density evolution of ellliptical galaxies. At the other end of the luminosity range, recent observations (Brown et al. 2007; Cool et al. 2008) indicate that the luminous $M_B - 5\log_{10} h \leq -21$ red galaxy population, loosely identified with ellipticals, were already in place at $z = 1$ whereas the corresponding model elliptical luminosity density, integrated between $-24.5 \leq M_K - 5\log_{10} h \leq -25.5$, shows an increase by a factor of 4 since $z = 1$. Thus, the model predicts significant evolution of the most luminous elliptical galaxies since $z = 1$ that observers do not see. One possible reason for the discrepancy is that the colour selection criteria employed by observers may result in significant contamination of the observational data sets with galaxies that are not actually ellipticals, causing elliptical galaxy evolution to be underestimated. This potential problem with the observations was

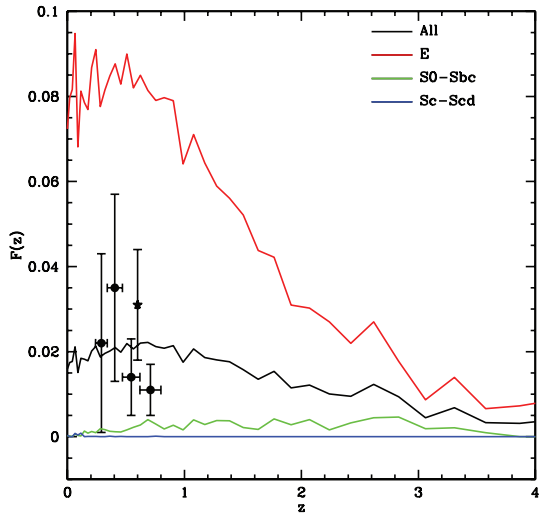

Figure 11. The fraction of galaxies with mass $>2.5 \times 10^{10}\,\mathrm{M}_{\odot}$ (corresponding to $M_{\mathrm{K}} - 5\log_{10} h \leq -22.7$) that have undergone a major merger ($M_2/M_1 > 0.25$) within the past 1 Gyr. The black line shows the predicted merger fraction averaged over all morphological types, while the blue, green and red lines show the predicted merger fraction for disc, disc+bulge and bulge morphological classes, respectively. Points show estimates of the merger fraction based on observations described by Jogee et al. (2009) and López-Sanjuan et al. (2009) (circles and star, respectively).

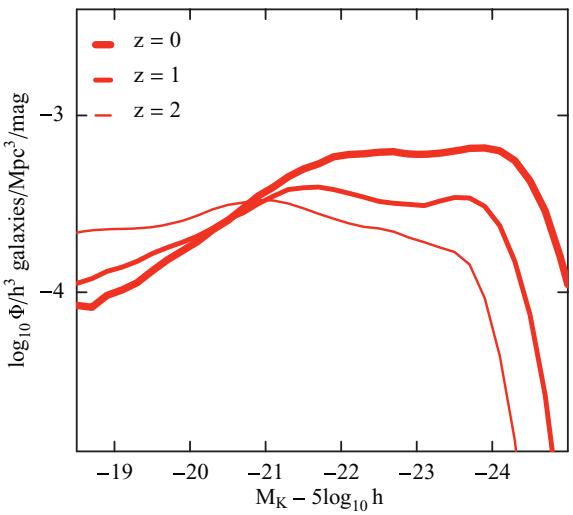

Figure 12. The predicted evolution of the elliptical galaxy LF with redshift. The LFs have been *k*-corrected and passively evolved to $z = 0$. So, the differences reflect the mass build up, primarily due to mergers at the high-luminosity end: $-24.5 \leq M_K - 5\log_{10} h \leq -25.5$.

noted previously by Faber et al. (2007). It is crucial therefore to understand the connection between the luminous red galaxy population seen at $z \sim 1$ and the elliptical population at $z = 0$. Are the luminous red galaxies seen at $z \sim 1$ the progenitors of today's ellipticals or are they dusty objects destined to become what we recognize in the local universe as lenticulars, or early-type spiral galaxies? Of course, another possibility is that the model may be at fault in overestimating the evolution of luminous ellipticals although, in defense of the model, it does succeed in predicting the observed space density of ellipticals at $z = 0$[7] and the observed type averaged merger rate (Section 4.1) and the observed star formation rate, as described in more detail in the next section.

4.3 The star formation history as a function of morphological type

With regard to elliptical galaxies, the results presented in Fig. 6 confirm the trend seen observationally (e.g. Thomas et al. 2005 and references therein) that the star formation redshift for elliptical galaxies is correlated with their mass (luminosity) in the sense that the stars comprising the more massive (luminous) ellipticals are old. The model predicts that half the stars comprising today's luminous, $-25 \leq M_{\mathrm{K}} - 5\log_{10} h \leq -24$, ellipticals formed between redshifts of 2 and 4 with ages $\sim$10 Gyr and were subsequently assembled via mergers, that occurred since $z \sim 3$, into the objects we recognize in the local universe as luminous elliptical galaxies. In contrast, stars comprising the lower luminosity, $-24 \leq M_{\mathrm{K}} - 5\log_{10} h$, ellipticals are younger with ages spanning 4–10 Gyr and were created in star formation episodes, the most recent of which were triggered by disc instabilities that occurred since $z \sim 2$. Thus, the seemingly antihierarchical behaviour depicted in Fig. 6 results from the fact that there are different mechanisms governing the star formation history of ellipticals: mergers for the luminous ones and disc instabilities for the less luminous ones. These results on formation redshift are insensitive to merger tree mass resolution (with galaxy mean stellar ages changing by only a few per cent if we increase the merger tree resolution by a factor of 16) and to the details of the treatment of disc instabilities (adopting the minimalistic model of Appendix A2 results in changes to mean stellar age of less than 10 per cent). We note that, in our model, the amount of mass brought in to low-luminosity ellipticals by minor mergers is relatively small due to the strong supernovae feedback which acts to suppress galaxy growth in lower mass haloes.

In Fig. 13, we compare model predictions concerning the evolution of the SSF rates with those measured recently by Pérez-González et al. (2008) for massive $\geq 10^{11}\,\mathrm{M}_{\odot}$ galaxies. The measured star formation rates are computed assuming a Chabrier initial mass function and so correspond to the total star formation rate (i.e. including stars of all masses). The same is predicted by the model (in which we compute the total star formation rate from the known dynamical time and gas content of each model galaxy). The principal merits of the Pérez-González et al. (2008) work are that the SSF rates are based on UV to mid-IR photometry and the results are segregated by visual morphology. The figure shows that the observed SSF rates for 'discy galaxies' and 'spheroids' are bounded by the model predictions for 'disc' and 'bulge+disc' galaxies and both the model and observations show a well-established trend that the SSF rate is decreasing with decreasing redshift, with implications for the stellar mass accumulated in these types of systems (Dahlen et al. 2007; Chen et al. 2009).

4.4 The secular evolution of bulges

The model predicts that the bulges in spiral galaxies have grown through a combination of disc instabilities and minor mergers.

[7]Since the parameters of the model were adjusted to match the observed morphologically segregated LFs, this is not strictly a prediction. However, the unadjusted Bower et al. (2006) model also yields a similar space density for elliptical galaxies as shown in Fig. 1.

Table 3. K-band LF fit parameters.

Sample	ϕ_*/h^3 (10^{-4} galaxies Mpc^{-3} mag^{-1})	$M_* - 5\log_{10} h$ (mag)	α	j ($10^7\, h\, \mathrm{L}_\odot\, \mathrm{Mpc}^{-3}$)
$z = 0$	16.1 ± 0.5	-23.93 ± 0.07	-0.48 ± 0.02	10.4
$z = 1$	7.1 ± 0.3	-23.77 ± 0.09	-0.70 ± 0.02	4.3
$z = 2$	4.9 ± 0.2	-23.15 ± 0.08	-0.82 ± 0.01	1.9

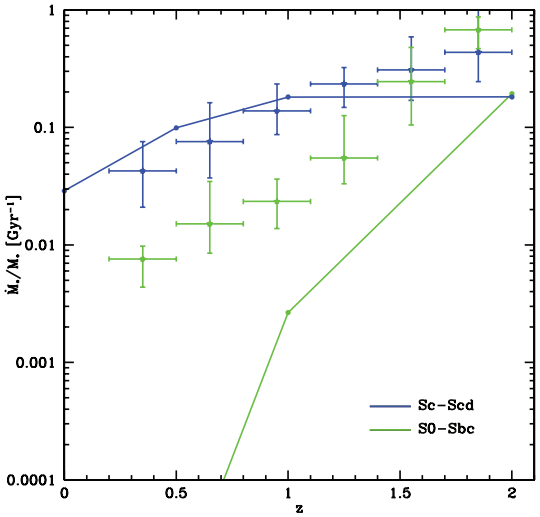

Figure 13. The evolution of the SSF rate with redshift for massive $\geq 10^{11}\,\mathrm{M}_\odot$ galaxies. The blue and red crosses identify the discy galaxies and spheroids of Pérez-González et al. (2008). The blue and green lines identify the model disc and disc+bulge galaxies, respectively. The model SSF rates for the bulge-dominated elliptical galaxies are essentially zero.

Observationally, the colour of bulges are more similar to the discs in which they reside than to other bulges (Balcells & Peletier 1994; Peletier & Balcells 1996). This coupling between bulge and disc colour has been observed out to $z \sim 1$ (Domínguez-Palmero & Balcells 2008, 2009) where younger, bluer high surface brightness bulges have been observed, suggesting an epoch of bulge formation. In concurrence with the observations, the model predicts that bulges in luminous $M_\mathrm{K} - 5\log_{10} h \sim -23$ spiral galaxies have grown significantly through a combination of disc instabilities and minor mergers since $z \sim 2$ and the model further predicts that bulges have been growing for a much longer time period, since $z \sim 4$, in lower luminosity systems.

5 CONCLUSIONS

The GALFORM semi-analytic model of galaxy formation (Bower et al. 2006) has been employed to reproduce and explain trends in galaxy morphology seen across a wide range of luminosities. Small adjustments to the model parameters permit excellent agreement with the observed morphologically selected K-band LF of Devereux et al. (2009), although the unmodified Bower et al. (2006) model also performs very well. While predicting morphology from semi-analytic models (and numerical simulations) remains challenging, a conservative approach has been adopted by categorizing model galaxies into just three broad classes: E ('pure spheroid'), S0-Sbc ('intermediate') and Sc-Scd ('pure disc') based on their K-band B/T luminosity ratio. Within this conservative categorization, the results presented are converged with respect to the resolution of the N-body-derived merger trees (see Appendix A1). Our conclusions follow.

(i) The Sc-Scd disc galaxies, with ∼10 per cent or less of their K-band light coming from the bulge, can form in abundance even in a hierarchical CDM cosmology in which merging is, in general, commonplace. The median merger history of the haloes that these galaxies inhabit is not significantly different from that of elliptical galaxies which do experience significant merging. However, the variation around that median history is much less for the Sc-Scd galaxies than for ellipticals. The Sc-Scd class typically experience a very simple accretion history, deviating little from the median and exhibiting relatively few large merging events. The formation history of these systems is therefore determined by the rate of growth of their dark matter halo and the corresponding rate of gas supply, cooling and infall. Galaxies in this class have typically been forming stars in their discs over large fractions of cosmic history and continue to do so at the present day. Dutton (2009) has suggested that producing bulgeless disc galaxies in sufficient numbers could be challenging in a CDM universe. In fact, because there is a sufficiently large number of dark matter haloes with relatively quiet merging histories, bulgeless disc galaxies can prevail, in the numbers observed. Additionally, strong feedback prevents the formation of relatively massive satellites around these galaxies which are predominantly low mass.

(ii) Luminous elliptical galaxies form through multiple mergers of smaller progenitors. For the most massive ellipticals these mergers tend to be 'dry' and so contribute no new star formation. Interestingly, the GALFORM model does not produce the dwarf elliptical sequence which should emerge at $M_\mathrm{K} - 5\log_{10} h \sim -21$ mag. Thus, the model prediction concerning the shape of the LF for low-luminosity ellipticals (with $M_\mathrm{K} - 5\log_{10} h > -21$ mag) and the model prediction that they form through disc instability events are uncertain.

(iii) The intermediate morphological types, S0-Sbc, are characterized by an early period of merging and disc instability events which form the bulge, followed by an extended period of steady, uninterrupted disc growth.

(iv) The model results concur with several observational results including the type averaged galaxy merger rate, measurements of the SSF rate, the secular evolution of spiral bulges, the seemingly antiheirarchical evolution of elliptical galaxies and the factor of ∼2 growth in the luminosity density of elliptical galaxies since $z \sim 1$. With regard to the last point however, the model predicts significant evolution at the high-luminosity end of the K-band elliptical galaxy LF that has yet to be confirmed observationally.

ACKNOWLEDGMENTS

AJB acknowledges support from the Gordon and Betty Moore Foundation and would like to acknowledge the hospitality of the KITP at the University of California, Santa Barbara, where part of this work

was completed. This research was supported in part by the National Science Foundation under Grant No. NSF PHY05-51164.

REFERENCES

Abraham R. G., Tanvir N. R., Santiago B. X., Ellis R. S., Glazebrook K., van den Bergh S., 1996, MNRAS, 279, L47
Agertz O., Teyssier R., Moore B., 2009, MNRAS, 397, L64
Balcells M., Peletier R. F., 1994, AJ, 107, 135
Barnes J. E., Hernquist L., 1992, ARA&A, 30, 705
Bell E. F., de Jong R. S., 2000, MNRAS, 312, 497
Bell E. F., McIntosh D. H., Katz N., Weinberg M. D., 2003, ApJS, 149, 289
Bell E. F. et al., 2004, ApJ, 608, 752
Benson A. J., Bower R. G., Frenk C. S., Lacey C. G., Baugh C. M., Cole S., 2003a, ApJ, 599, 38
Benson A. J., Frenk C. S., Baugh C. M., Cole S., Lacey C. G., 2003b, MNRAS, 343, 679
Bertone S., Conselice C. J., 2009, MNRAS, 396, 2345
Blanton M. R., 2006, ApJ, 648, 268
Bower R. G., Benson A. J., Malbon R., Helly J. C., Frenk C. S., Baugh C. M., Cole S., Lacey C. G., 2006, MNRAS, 370, 645
Brown M. J. I., Dey A., Jannuzi B. T., Brand K., Benson A. J., Brodwin M., Croton D. J., Eisenhardt P. R., 2007, ApJ, 654, 858
Chen Y., Wild V., Kauffmann G., Blaizot J., Davis M., Noeske K., Wang J., Willmer C., 2009, MNRAS, 393, 406
Christodoulou D. M., Shlosman I., Tohline J. E., 1995, ApJ, 443, 551
Cole S., Lacey C. G., Baugh C. M., Frenk C. S., 2000, MNRAS, 319, 168
Cool R. J. et al., 2008, ApJ, 682, 919
Croton D. J. et al., 2006, MNRAS, 365, 11
Dahlen T., Mobasher B., Dickinson M., Ferguson H. C., Giavalisco M., Kretchmer C., Ravindranath S., 2007, ApJ, 654, 172
de Vaucouleurs G., 1959, Handbuch der Physik, 53, 275. Springer, Berlin
de Vaucouleurs G., de Vaucouleurs A., Corwin H. G., Buta R. J., Paturel G., Fouque P., 1991, Third Reference Catalogue of Bright Galaxies. Springer, Berlin
Devereux N. A., Becklin E. E., Scoville N., 1987, ApJ, 312, 529
Devereux N., Willner S. P., Ashby M. L. N., Willmer C. N. A., Hriljac P., 2009, ApJ, 702, 955
Domínguez-Palmero L., Balcells M., 2008, A&A, 489, 1003
Domínguez-Palmero L., Balcells M., 2009, ApJ, 694, L69
Dutton A. A., 2009, MNRAS, 396, 121
Efstathiou G., Lake G., Negroponte J., 1982, MNRAS, 199, 1069
Faber S. M. et al., 2007, ApJ, 665, 265
Fakhouri O., Ma C., 2009, MNRAS, 394, 1825
Genel S., Genzel R., Bouché N., Naab T., Sternberg A., 2009, ApJ, 701, 2002
Graham A. W., Worley C. C., 2008, MNRAS, 388, 1708
Harker G., Cole S., Helly J., Frenk C., Jenkins A., 2006, MNRAS, 367, 1039
Hatton S., Devriendt J. E. G., Ninin S., Bouchet F. R., Guiderdoni B., Vibert D., 2003, MNRAS, 343, 75
Hopkins P. F., Cox T. J., Keres D., Hernquist L., 2008, ApJS, 175, 390
Hubble E. P., 1936, Realm of the Nebulae. Yale Univ. Press, New Haven
Jogee S. et al., 2009, ApJ, 697, 1971
Lacey C., Cole S., 1993, MNRAS, 262, 627
López-Sanjuan C. et al., 2009, ApJ, 694, 643
Lotz J. M., Primack J., Madau P., 2004, AJ, 128, 163
Mandelbaum R., Seljak U., Cool R. J., Blanton M., Hirata C. M., Brinkmann J., 2006, MNRAS, 372, 758
Mandelbaum R., Li C., Kauffmann G., White S. D. M., 2009, MNRAS, 393, 377
Masjedi M., Hogg D. W., Blanton M. R., 2008, ApJ, 679, 260
Oppenheimer B. D., Davé R., 2006, MNRAS, 373, 1265
Parkinson H., Cole S., Helly J., 2008, MNRAS, 383, 557
Parry O. H., Eke V. R., Frenk C. S., 2009, MNRAS, 396, 1972
Peletier R. F., Balcells M., 1996, AJ, 111, 2238
Pérez-González P. G., Trujillo I., Barro G., Gallego J., Zamorano J., Conselice C. J., 2008, ApJ, 687, 50
Ratnatunga K. U., Griffiths R. E., Ostrander E. J., 1999, AJ, 118, 86
Schade D., Carlberg R. G., Yee H. K. C., Lopez-Cruz O., Ellingson E., 1996, ApJ, 464, L63
Simard L. et al., 2002, ApJS, 142, 1
Springel V. et al., 2005, Nat, 435, 629
Stewart K. R., Bullock J. S., Wechsler R. H., Maller A. H., Zentner A. R., 2008, ApJ, 683, 597
Stewart K. R., Bullock J. S., Barton E. J., Wechsler R. H., 2009, ApJ, 702, 1005
Strateva I. et al., 2001, AJ, 122, 1861
Thomas D., Maraston C., Bender R., de Oliveira C. M., 2005, ApJ, 621, 673
Watanabe M., Kodaira K., Okamura S., 1985, ApJ, 292, 72
Weinberg D. H., Dav R., Katz N., Hernquist L., 2004, ApJ, 601, 1
Willmer C. N. A. et al., 2006, ApJ, 647, 853

APPENDIX A: ROBUSTNESS OF MODEL MORPHOLOGIES

In this appendix, we explore the effects which could influence the morphological properties of model galaxies, and demonstrate that, in fact, our results are robust to these effects.

A1 Resolution study

Since morphological evolution in our model is driven at least partly by merging activity, it is important to assess whether the resolution of the N-body merger trees that we utilize causes us to miss some lower mass merging activity and, therefore, to incorrectly estimate morphologies of some galaxies. While we currently do not have suitable N-body merger trees with higher resolution available to us for a resolution study, we can instead utilize merger trees constructed using a modified extended Press–Schechter approach (see Parkinson, Cole & Helly 2008) which is designed to produce trees which are statistically equivalent to those found in N-body simulations. The advantage of this approach is that it allows us to increase the resolution to almost arbitrarily high levels. While the results will not precisely match those obtained using N-body trees, they are sufficiently close to allow us to explore the effects of changing resolution. Fig. A1 below shows the results of a resolution study carried out in this way on the morphologically segregated LF.

The thickest lines correspond to the case of N-body merger trees drawn from the Millennium Simulation (i.e. used in this paper). The remaining lines were all generated using the exact same model parameters but with merger trees constructed using the Parkinson et al. (2008) algorithm. Of these lines, the thickest has a resolution matched to that of the Millennium Simulation. As can be seen (Fig. A1), it does not produce LFs in precise agreement with those obtained using Millennium Simulation merger trees (since the analytic merger trees are not exactly statistically equivalent to the N-body ones), but they are very close. The thinner lines represent results obtained when the mass resolution in the analytic merger trees is increased (i.e. shifted to smaller masses) by factors of 4 and 16. It can clearly be seen that there is no significant change in the predicted LFs. As such, we conclude that galaxy morphologies are well converged in our model when using trees with the Millennium mass resolution. (This is a consequence of the effects of supernovae feedback, which makes galaxy formation in lower mass haloes highly inefficient and, therefore, to have little effect on more massive galaxies.)

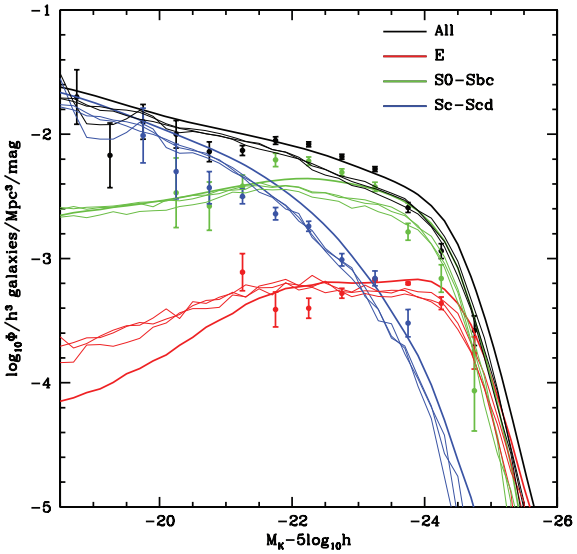

Figure A1. A study of resolution effects on the morphologically segregated LF of Fig. 1. The thickest lines show the results obtained utilizing Millennium Simulation merger trees (i.e. as used throughout our work). The remaining three sets of lines were produced using analytically generated merger trees (using the algorithm of Parkinson et al. 2008). The thickest of these lines correspond to analytic trees with a mass resolution matched to that of the Millennium Simulation, while successively thinner lines have 4 and 16 times better mass resolution.

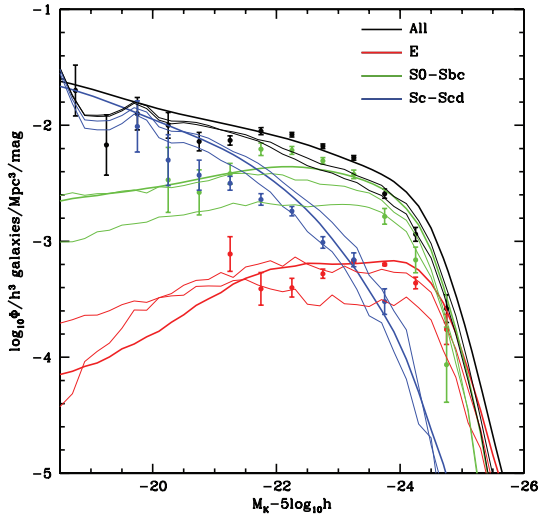

Figure A2. The effects of an alternative disc instability model on the morphologically segregated LF. The thickest lines show results from our standard treatment of disc instabilities applied to merger trees extracted from the Millennium Simulation. Intermediate lines indicate the same standard treatment of instabilities but applied to analytically derived merger trees (using the algorithm of Parkinson et al. 2008). Finally, the thinnest lines show the results of adopting an alternative treatment of disc instabilities (in which only just enough mass is transferred from an unstable disc to cause it to restabilize) applied to analytically derived merger trees.

A2 Alternative treatment of disc instabilities

The instability of galaxy discs is a difficult process to treat analytically. Our standard approach assumes that any unstable disc will quickly develop a strong bar and destroy itself entirely, turning the galaxy into a pure spheroid. Recent, high-resolution hydrodynamical simulations (Agertz, Teyssier & Moore 2009) show that unstable discs experience local instabilities leading to fragmentation and the incomplete destruction of the disc. To at least partially assess the importance of the assumptions we make regarding disc instabilities, we have implemented an alternative disc instability treatment in our model in which only just enough mass is transferred from the disc to the spheroid component to restabilize the disc – an approach which has been adopted by other semi-analytic models (Hatton et al. 2003; Croton et al. 2006). Fig. A2 shows the effect of switching to this alternative treatment on the morphologically segregated LF. The thickest lines show results utilizing Millennium Simulation trees with our standard treatment of disc instabilities. Medium thickness lines show the same treatment of instabilities but with analytic merger trees with resolution matched to that of the Millennium Simulation. Finally, the thinnest lines show results of using the alternative treatment of instability events with analytic merger trees.

The net result of switching to the alternative treatment of instabilities is to slightly increase the number of bulgeless galaxies at all luminosities, with a corresponding decrease in the numbers of intermediate and pure spheroid galaxies. The changes do not alter the qualitative trends of morphological mix with luminosity. However, in order to reproduce quantitatively the observed morphological mix of galaxies at $M_{\rm K} - 5\log h = -23$ would require adjusting the range of B/T used to segregate galaxies into the three broad morphological classes (Table 1). The sense of the required adjustment for the E ('pure spheroid') class would be to smaller B/T, which is inconsistent with their observed morphology and may be a sign that our standard treatment of disc instabilities is more realistic.

This paper has been typeset from a TEX/LATEX file prepared by the author.